AIP | Review of Scientific Instruments

NAIS: Nuclear activation-based imaging spectroscopy

M. M. Günther, A. Britz, R. J. Clarke, K. Harres, G. Hoffmeister, F. Nürnberg, A. Otten, A. Pelka, M. Roth, and K. Vogt

Citation: Review of Scientific Instruments **84**, 073305 (2013); doi: 10.1063/1.4815826
View online: http://dx.doi.org/10.1063/1.4815826
View Table of Contents: http://scitation.aip.org/content/aip/journal/rsi/84/7?ver=pdfcov
Published by the AIP Publishing

NAIS: Nuclear activation-based imaging spectroscopy

M. M. Günther,[1,a)] A. Britz,[1] R. J. Clarke,[2] K. Harres,[1] G. Hoffmeister,[1] F. Nürnberg,[1] A. Otten,[1] A. Pelka,[1] M. Roth,[1] and K. Vogt[3]
[1]*Institut für Kernphysik, Schlossgartenstr. 9, Technische Universität Darmstadt, D-64289 Darmstadt, Germany*
[2]*Central Laser Facility, Rutherford Appelton Laboratory, Chilton, Didcot, Oxon OX11 0QX, United Kingdom*
[3]*GSI – Helmholtzzentrum für Schwerionenforschung GmbH, D-64291 Darmstadt, Germany*

(Received 4 April 2013; accepted 1 July 2013; published online 22 July 2013)

In recent years, the development of high power laser systems led to focussed intensities of more than 10^{22} W/cm^2 at high pulse energies. Furthermore, both, the advanced high power lasers and the development of sophisticated laser particle acceleration mechanisms facilitate the generation of high energetic particle beams at high fluxes. The challenge of imaging detector systems is to acquire the properties of the high flux beam spatially and spectrally resolved. The limitations of most detector systems are saturation effects. These conventional detectors are based on scintillators, semiconductors, or radiation sensitive films. We present a nuclear activation-based imaging spectroscopy method, which is called NAIS, for the characterization of laser accelerated proton beams. The offline detector system is a combination of stacked metal foils and imaging plates (IP). After the irradiation of the stacked foils they become activated by nuclear reactions, emitting gamma decay radiation. In the next step, an autoradiography of the activated foils using IPs and an analysis routine lead to a spectrally and spatially resolved beam profile. In addition, we present an absolute calibration method for IPs.
 [http://dx.doi.org/10.1063/1.4815826]

I. INTRODUCTION

Nowadays, laser systems are able to reach maximum focussed intensities[1,2] of more than 10^{22} W/cm^2. The interaction of these ultra intense laser beams with matter accelerates electrons close to the speed of light. Most applications using high-intense lasers are driven by the relativistic electrons. The investigation of relativistic laser-matter interactions is the basis to perform these applications efficiently. To learn more about the interaction processes or mechanisms, it is mandatory to characterize the electron dynamics at the interaction region. In the past few years, several diagnostic methods were developed for the investigation of relativistic laser-matter interactions.[3,5–8]

One important application is the laser-ion acceleration. A well known acceleration mechanism is the *Target Normal Sheath Acceleration* (TNSA).[9] This acceleration mechanism is induced by a rapid charge separation, which forms an electron sheath on target rear surface.[4] The resulting electric field on the rear-side exceeds 10^{12} V/m. The strong electric field leads to field ionisation mostly of hydrogen consisting in impurities at the target rear surface. The ionized protons are accelerated normal to the surface along the electric field lines. The TNSA mechanism has been investigated well since the last decade. This acceleration mechanism typically leads to a quasi-thermal energy distribution of protons with energies of several tenth of MeV and particle numbers of more than 10^{13}. Recent discussions have proposed new acceleration mechanisms based on ultra high-intense laser-matter interactions.[10,11] The aim is to push the number of ions and the energy, respectively. Furthermore, in some applications it is desirable to produce more monoenergetic particle spectra.

The important advantages regarding laser-accelerated ions compared to conventionally accelerated ion beams are the low transverse emittance, the high brightness, and the short pulse duration. There are various potential applications in nuclear science, the realization of a laser driven neutron source, medical applications, radiography, and the next generation ion source for injection into conventional accelerators. For these applications, it is mandatory to control the beam parameters for the generation and optimization concerning source size, divergence, transverse emittance, and the spatial and energy resolved distribution.

Recently, several techniques were discussed or used to characterize laser-accelerated ion or proton beams. A well-established technique to characterize proton beams is the use of radiochromic films (RCF).[12] An experimental method to reconstruct beam parameters is the so-called radiochromic film imaging spectroscopy (RIS) by Nürnberg *et al.*[13] Further techniques are based on nuclear activations. In the past few years, proton-induced reactions in copper were discussed as a potential diagnostics application.[17] Furthermore, Tarisien *et al.*[15] used a nuclear activation based diagnostics system, which is called NATALIE, for the characterization of laser produced energetic particles. These techniques use the β^+ decay of activated isotopes to reconstruct the energy dependent reaction yield and thus to reconstruct the initial particle energy spectrum. To measure the decay via the annihilation radiation, NaI-detectors were used. The RIS method has two major disadvantages: The detector is used only one time, i.e., one detector per single laser shot. The consequence is a high consumption of RCFs concerning the next generation high-intense lasers with high rate of repetition. The second disadvantage is that the optical density of RCF

a)Electronic mail: m.guenther@gsi.de. Current address: GSI Helmholtzzentrum für Schwerionenforschung GmbH, Planckstrasse 1, D-64291 Darmstadt, Germany.

TABLE I. The most proton-induced nuclear reactions with copper in the natural abundance.[16] E_{th} is the nuclear reaction threshold. σ_{max} means the maximum reaction cross section at the energy $E(\sigma_{max})$.

Reaction	Decay type	Half-life	E_{th} (MeV)	σ_{max} (mb)	$E(\sigma_{max})$ (MeV)
^{63}Cu(p,2n)^{62}Zn	$\epsilon + \beta^+$	9.186 h	13.26	135	23
^{63}Cu(p,n)^{63}Zn	$\epsilon + \beta^+$	38.47 min	4.149	500	13
^{65}Cu(p,n)^{65}Zn	$\epsilon + \beta^+$	244.26 d	2.134	760	10.9
^{63}Cu(p,p+2n)^{61}Cu	$\epsilon + \beta^+$	3.333 h	19.74	323	40
^{65}Cu(p,p+n)^{64}Cu	$\epsilon + \beta^+, \beta^-$	12.7 h	9.91	490	25

irradiated by high proton fluxes is saturated. In addition, the RCF detector system could be destroyed by extreme high particle fluxes. Recently, a scintillator-based online detection system was developed for high repetition rate.[14] It can be used in low flux and high repetition rate applications. However, the limit could appear at laser generated high energy, high flux proton beams. Most applicable and efficient are nuclear activation-based diagnostic techniques to characterize laser-accelerated protons with high fluxes. Conventional nuclear diagnostics use scintillation-based detectors or semiconductor-based detector systems. An irradiated and activated sample is scanned in terms of the radioactive decay of activated sample isotopes using these detectors. The advantage is the reconstruction of the absolute yield of initial particles without saturation effects at high fluxes. A serious disadvantage of these conventional nuclear diagnostics compared to the RCF-based technique is that the reconstruction of the proton beam with high spatial and energetic resolution is not possible.

We present a nuclear activation-based imaging spectroscopy (NAIS) technique. This technique is very simple to use and practicable as well as efficient in beam characterization compared to earlier or other more sophisticated nuclear diagnostic methods. The proton detector consists of stacked foils of copper of natural abundance. The characterization of proton beams is performed by an autoradiography of activated copper foils using imaging plate (IP) detectors. The result of the autoradiography analysis is the spectrally and spatially resolved reconstruction of the beam profile. In Sec. II, the NAIS detector system and the IP calibration are presented. The spectral and spatial resolved beam reconstruction is processed in Sec. III. In addition, in this section exemplary results by NAIS are compared to results of RIS.

II. THE NAIS DETECTOR SYSTEM

The proton detector consists of stacked foils of copper of natural abundance. The stacked configuration allows an energetic and spatially resolved measurement. Each foil in the stack is related to an energy bin. To calculate the energy loss and Bragg peak energies in different thick and material foil layers, the SRIM code[21] (Stopping and Range of Ions in Matter) based on Monte Carlo simulation method was used. The protons of lower energy are stopped in the first layers and the protons with higher energies are stopped in the rear copper foils. Then, each copper foil becomes activated according to the energy of the protons. An autoradiography of the activated copper foils was performed using IPs for the spatial and spectral reconstruction of the beam profile. Within the IP photo-sensitive compounds are excited by the decay radiation of the activated isotopes of the copper foils. During the scanning process, photostimulated luminescence (PSL) radiation is emitted. The PSL value is related to the activity within the copper foils and, therefore, it is related to the proton-induced nuclear reaction yield. With the known reaction yield and the energy dependent reaction cross section, the number of laser accelerated protons can be reconstructed. The usage of the IP as detector for measuring the spatial and spectral distribution of protons demands the calibration of the IP concerning the decay radiation. This will be described below.

A. Proton-induced nuclear reactions in copper

We used copper in the natural abundance: That means 69.17% of ^{63}Cu and 30.83% of ^{65}Cu. The most nuclear reactions induced by protons with energies up to 100 MeV are shown in Table I.

The corresponding nuclear reaction cross sections are shown in Fig. 1. The ^{65}Cu(p,n)^{65}Zn reaction features the highest value of cross section. The value of the cross section of the ^{63}Cu(p,n)^{63}Zn reaction is below the cross section by the ^{65}Cu(p,n)^{65}Zn reaction. However, the half-life of ^{63}Zn is around 40 min, compared to the half-life of ^{65}Zn which is much bigger. That means the activity of ^{63}Zn produced in ^{63}Cu(p,n)^{63}Zn is much higher than the activity of ^{65}Zn. According to the radiation time of the IP directly after the copper activation, the decay of ^{63}Zn becomes dominant.

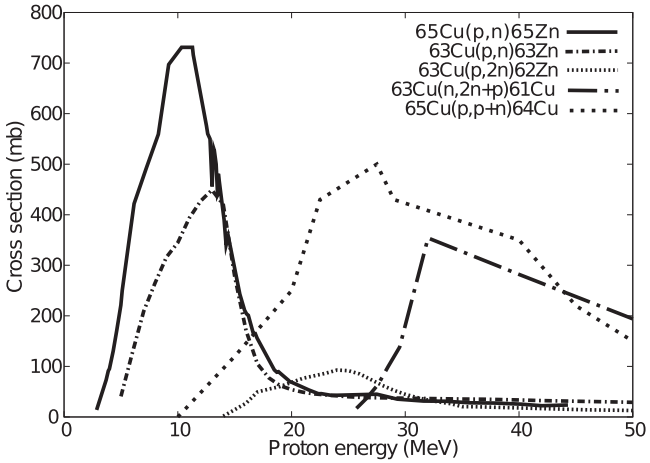

FIG. 1. The proton-induced nuclear reaction cross section in copper for different reaction types.[16]

The energy of the laser accelerated protons reaches several tenth of MeV. Thus, the initial numbers of activated nuclei within the copper foil are different according to the proton-induced reaction type. Therefore, the allover activity of the activated foil results from the sum of the activity of each activated isotope produced in several nuclear reactions listed in Table I. For the absolute calibration of the IP, it is necessary to know the reaction yield of each proton-induced nuclear reaction. The reaction yield can be determined using a gamma spectroscopy of an activated copper foil. Yang *et al.*[17] have measured the gamma decay spectrum of an activated copper sample which was irradiated by laser accelerated protons. The maximum proton energy was around 30 MeV. A typical proton spectrum of laser accelerated protons via the TNSA mechanism can be assumed as an exponentially decreasing distribution. Yang *et al.*[17] have determined that the ^{63}Cu(p,n)^{63}Zn and ^{65}Cu(p,n)^{65}Zn reaction yields were dominant.

In case of using a stack of copper foils, it is inefficient to perform a gamma spectroscopy for each foil. The autoradiography method using IPs is used within the first hour after the laser shot. To analyze the decay of the activated isotopes, we used a coincidence system. We used two NaI detectors with an aperture of 2 in. The detector system counts coincidently the contrary propagated annihilation photons at 511 keV which are due to the β^+ decay of the activated isotopes. The coincidence system has been calibrated using a ^{22}Na calibration source. Figure 2 shows the exemplary decay curve of four activated copper foils. The stack configuration which has been used is seen as a schematic in Fig. 3. We used alternating layers of RCF and copper within the stack. That enables the comparison between the RIS and the NAIS method. In this example, the maximum proton energy was around 24 MeV. The thickness of each copper foil is 50 μm. The first four copper foils were analyzed with the coincidence counting system. That means the Bragg peak deposition for protons in the first four copper layers is in the sequence of 5 MeV, 8 MeV, 11 MeV, and 15 MeV. The analysis of the count rate in the first hour results in a half-life of (40 $\pm$ 2) min. This half-life can be identified with the decay of the ^{63}Zn isotope from the ^{63}Cu(p,n)^{63}Zn reaction. Furthermore, it can be observed that the activity decreases with time. This is significant in case of the fourth copper layer. A change in the slope after the first hour of measure time is observed. That means there is an increasing of the half-life. It can be explained as follows: In the fourth layer, the maximum Bragg peak deposition is in the range of 15 MeV. The reaction threshold of the ^{63}Cu(p,2n)^{62}Zn reaction is at 13 MeV. That means above the threshold this reaction type is dominant instead of the ^{63}Cu(p,n)^{63}Zn reaction with a half-life of 38.47 min for ^{63}Zn. The half-life of ^{62}Zn is about 9 h. The counting of coincidence events over a longer period results in a higher half-life. The decay analysis in the first hour after the laser shot leads to the result that the ^{63}Cu(p,n)^{63}Zn reaction type is dominant.

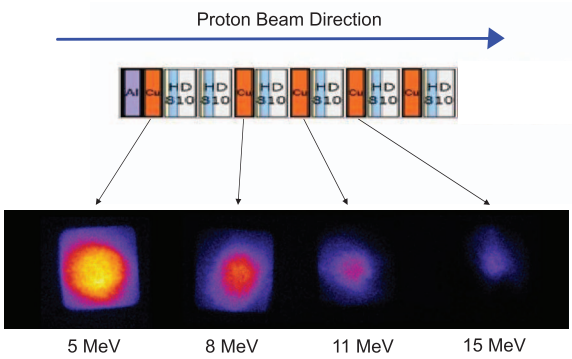

FIG. 3. Schematic of a stack of alternating layers of RCF and copper foils. Below is the autoradiography of activated copper foils using IPs. The energies mean the minimum incidence energies of protons which are necessary for proton induced nuclear reactions in each copper layer.

Figure 4 demonstrates a gamma decay spectrum of an activated copper stack. The stack was irradiated by laser accelerated protons. The number of protons was above 10^{13} and the maximum proton energy was 30 MeV. The observed gamma decay lines result from the activated isotopes produced in the

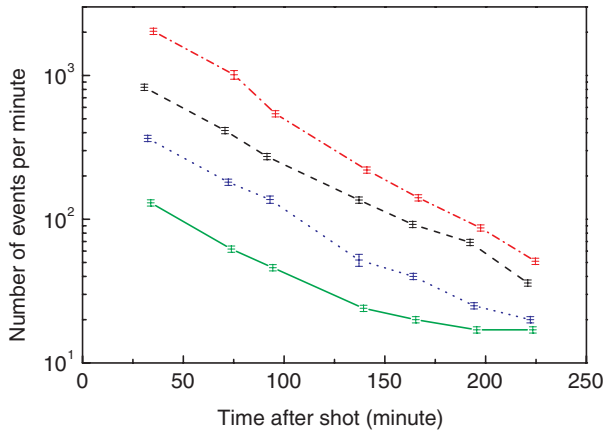

FIG. 2. Decay curves of four activated copper foils of the stack. The first dashed-dotted line denotes the first copper layer, the dashed line the second, the dotted line the third, and the continuous line the fourth layer.

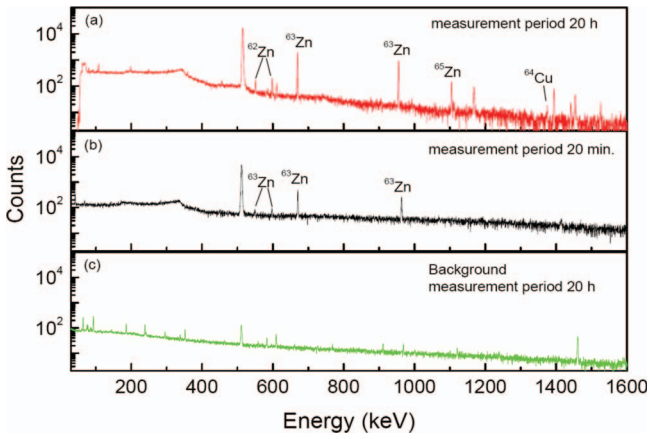

FIG. 4. Gamma-ray decay spectrum after proton-induced activation of the copper foils. The protons were produced by a PHELIX shot. The number of protons was 10^{13} and the maximum energy of the protons was 30 MeV. The upper panel (a) shows the gamma decay spectrum after a measure time of 20 h. (b) shows the spectrum after 20 min according to the time in which the autoradiography is performed. The lower panel (c) denotes the background spectrum of the used high purity germanium detector after 20 h.

following proton-induced nuclear reactions: ^{65}Zn is produced in the ^{65}Cu(p,n)^{65}Zn reaction. This reaction has the largest cross section (see Fig. 1). However, the activity is several orders of magnitude less than the activity of the isotope ^{63}Zn produced in the ^{63}Cu(p,n)^{63}Zn reaction. This is because the half life of ^{65}Zn is 244 days and the natural abundance of the initial isotope ^{65}Cu (30.83%) is less than the natural abundance of ^{65}Cu. The consequence is that the fraction of activity concerning the allover activity of the activated copper foils is negligibly small. Furthermore, ^{64}Cu is identified which is produced in the ^{65}Cu(p,p+n)^{64}Cu reaction. The fraction of activity with respect to the general activity is also negligibly small. ^{62}Zn is produced in the ^{63}Cu(p,2n)^{62}Zn reaction and can be identified during the first 20 min of measurement. The allover activity of the activated copper foils is about 5%. The largest fraction of the activity regarding the overall activity arose from the decay of ^{63}Zn. Therefore, we used the ^{63}Cu(p,n)^{63}Zn reaction type for the IP calibration.

B. IP calibration

A cross-calibration is used for the absolute calibration of the IPs. Using a coincidence counting system, the ^{63}Cu(p,n)^{63}Zn reaction yield was obtained. It should be noted that the counting measurement of the activated copper foils is within the time t_1 and t_2 ($t_1 < t_2$) after the laser shot. To determine the activity C_0 directly after the shot ($t = 0$), the decay law was used

$$C(t_1, t_2) = \int_{t_1}^{t_2} \lambda C_0 \exp(-\lambda t) dt. \quad (1)$$

$C(t_1, t_2)$ are the counts between t_1 and t_2, and λ is the radioactive constant regarding the decay of ^{63}Zn. Thus, the activity at $t = 0$ is

$$C_0 = \frac{C(t_1, t_2)}{\tau(t_1, t_2)}, \quad (2)$$

where $\tau(t_1, t_2)$ is the time correction factor

$$\tau(t_1, t_2) = (e^{-\lambda t_2} - e^{-\lambda t_1})^{-1}. \quad (3)$$

The reaction yield Y_0 is obtained as follows via Eq. (2):

$$Y_0 = \frac{C(t_1, t_2)}{0.93 \cdot \epsilon_{coinc} \tau(t_1, t_2)}, \quad (4)$$

where ϵ_{coinc} means the efficiency of the coincidence detection system. In addition, Eq. (4) contains the branching ratio related to the β^+ decay channel, which is about 93%.

Furthermore, for the autoradiography of the activated copper foils we used the IP type MM 3.0 without protecting layer from AGFA. The IPs were irradiated in the measure time of 20 min. For the IP scanning process, we have used the scanner type FLA7000 from Fuji. For the calibration of the IPs, the overall number of photostimulated luminescence emitted during the scanning process is used for each foil. The comparison of the PSL value with the reaction yield Y_0 of ^{63}Zn leads to the calibration of the IP. The autoradiograph of each copper foil can be analyzed using an analyzing routine. The result of the analysis is an array of PSL values per pixel. To obtain the overall PSL number, the PSL values within the array have been added. Furthermore, the background PSL value was subtracted from the overall PSL value. In addition, on the lines of the coincidence counting measurement using the decay law, the PSL value has to count back to the time of activation. Using the efficiency ϵ_{IP} of the IP, the whole number of copper activations is given by

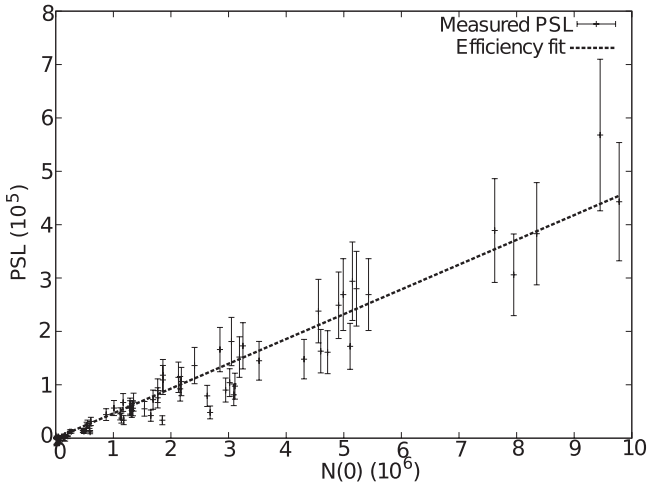

FIG. 5. PSL value as a function of the proton induced nuclear reaction yield. The slope of the line of best fit (dashed line) denotes the efficiency of the IP. Used IP type: MM 3.0 without protecting layer from AGFA.

$$N(0) = \frac{PSL(t_1, t_2)}{\tau(t_1, t_2)\epsilon_{IP}}. \quad (5)$$

But, the IP efficiency ϵ_{IP} is not known. The number of activations $N(0) = Y_0$ is well-known from the coincidence counting measurement, also the time correction factor $\tau(t_1, t_2)$ is known. Therefore, the IP efficiency can be written as

$$\epsilon_{IP} = \frac{PSL(t_1, t_2)}{\tau(t_1, t_2)N(0)}. \quad (6)$$

To determine the IP efficiency, the PSL value is compared to the number of activations. The comparison and therefore the cross-calibration is shown in Fig. 5. The relation between the PSL value and the number of activations from each foil is linear. A linear fit leads to the value of the IP efficiency of the used IP type. The efficiency is given by $\epsilon_{IP} = (46.4 \pm 1.2) \times 10^{-3}$ PSL.

III. SPECTRALLY AND SPATIALLY RESOLVED BEAM RECONSTRUCTION

With the known IP calibration, a quantitative proton beam characterization is available using the nuclear activation of copper foils. For the comparison of NAIS with the conventional proton detection method RIS, a stack of alternating copper foils and RCFs is used (a schematic is shown in Fig. 6). Also, the spatial distribution of laser-accelerated protons can be quantitatively reconstructed using an autoradiography of activated copper foils together with the IP calibration curve. Fig. 7 shows the spatial distribution of protons according to the proton energy given by each copper layer. In the stack, 16 copper layers are used but only the first 11 layers are

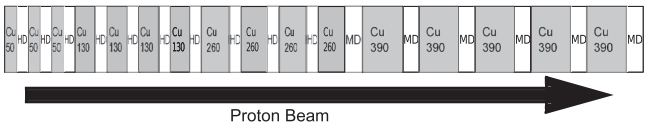

FIG. 6. Schematic of the stack of alternating copper foils and RCF. Copper foils are used with different thicknesses (50, 130, 260, and 390 μm). RCFs are used with different sensitivities (MD is more sensitive regarding the protons).

activated. This is because the maximum incidence proton energy is too low for penetrating the whole stack totally.

To deconvolve the proton spectrum from copper activations, we used an analysis routine based on MATLAB.[18] The routine also contains the IP calibration curve shown in Fig. 5. The mathematics is described as follows.

The yield function of proton induced nuclear reactions in copper of the kth layer is given by

$$Y(k) = \int_{E_{th}}^{E_{max,k}} Q(E', k)\frac{dN_p}{dE}(E')dE', \tag{7}$$

where $Q(E', k)$ contains the properties of the kth copper foil and the energy dependent nuclear reaction cross-section $\sigma(E')$. $\frac{dN_p}{dE}(E')$ is the proton spectrum. For the numerical integration, Eq. (7) can be written as the sum over i sufficiently small energy bins ΔE_i,

$$Y(k) = \sum_i Q(E_i', k)\frac{dN_p}{dE}(E_i')\Delta E_i'. \tag{8}$$

The energy bins are small enough, so that the number of protons can be assumed to be constant for each energy interval. Therefore, the reaction cross section in these intervals is constant. The choice for the energy bin depends on the reaction threshold for ^{63}Cu(p,n)^{63}Zn which is 4.15 MeV. That means there is a minimum energy for which the protons propagate the foil stack. In addition, the energies for the bth energy bin is given by $E_{b,0}$, where 0 means the energy before the stack. The energy bins can be considered as the averaged energies

$$\bar{E}_{b,0} = \frac{E_{(b+1),0} + E_{b,0}}{2}. \tag{9}$$

Therefore, the interval is given by $\Delta\bar{E}_{b,0} = E_{(b+1),0} - E_{b,0}$. The number of protons within the energy interval is $N_{p,b} = \frac{dN_p}{dE}(\bar{E}_{b,0})\Delta\bar{E}_{b,0}$. Furthermore, the proton energy from the bth energy bin amounts in the kth foil $\bar{E}_{b,k}$. The count of the energy bins is from the lowest to the highest energy. That means the index of each foil rises with the propagation direction of the protons through the stack. For the bth energy bin within the kth copper layer, the overall cross section can be written as

$$Q(\bar{E}_{b,k}, k) = I_{\%}\frac{\sigma(\bar{E}_{b,k})N_A\rho_{Cu}d_{layer}(k)}{M}. \tag{10}$$

Here, $I_{\%}$ is the fraction of the copper isotope, $\sigma(\bar{E}_{b,k})$ is the energy dependent reaction cross section, N_A is the Avogadro's constant, ρ_{Cu} the mass density of copper, $d_{layer}(k)$ the thickness of the kth copper layer, and M the molar mass of elementary copper.

Then, according to Eq. (8) the number of protons per energy bin b can be written as

$$Y(k) = \sum_b Q(\bar{E}_{b,k}, k)\frac{dN_p}{dE}(\bar{E}_{b,0})\Delta\bar{E}_{b,0}. \tag{11}$$

The energy bins $\Delta\bar{E}_{b,0}$, and the reaction yield of the kth foil $Y(k)$ as well as the reaction cross section, and the foil properties $Q(\bar{E}_{b,k}, k)$ are well known. The yield $Y(k)$ can be determined using the autoradiography via the absolute calibration of the IPs. Equation (11) describes a linear system of equations (LSE). The LSE can be solved according to Penfold and Leiss[19] for the number of protons per energy bin by varying the intervals of the energy bins and the reaction cross section. These bins are given by the thickness of copper foils and the stack configuration. In general, we used a fit method for the deconvolution of the proton spectrum, because the choice of energy bins was rough, e.g., for the comparison with the RIS method we used RCFs between the copper layer which leads to an increase of each energy bin, and therefore a decrease in inaccuracy for solving the LSE. Furthermore, within the large energy bins the reaction cross sections have a wide variation which also leads to inaccuracy in solving procedure. For applications using a stack of several thin copper foils only, the energy bins become small and the variation of the cross section within the energy bin is low. In that case, it allows for exact deconvolution of the proton spectrum using the Penfold-Leiss method.

The spectrum of accelerated protons via the TNSA mechanism can be described using an exponential spectrum given by

$$\frac{dN_p}{dE} = \frac{N_{p,0}}{E_p}\exp\left(-\frac{E_p}{k_BT}\right). \tag{12}$$

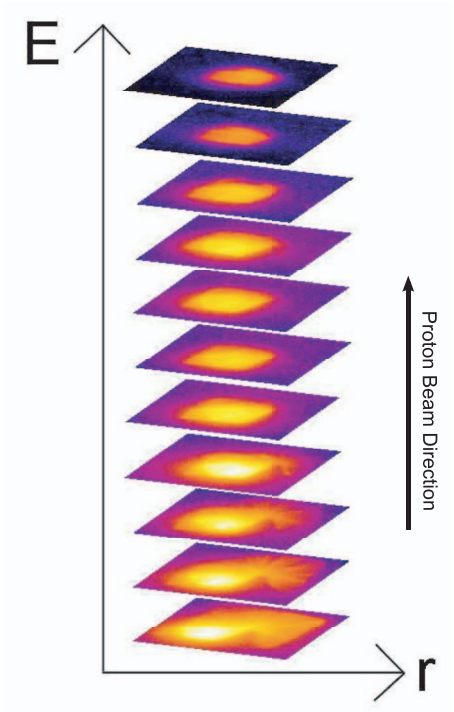

FIG. 7. Spatial distribution of protons according to the energy given by each copper layer. The color gradient indicates low particle number (blue) up to high particle number (yellow).

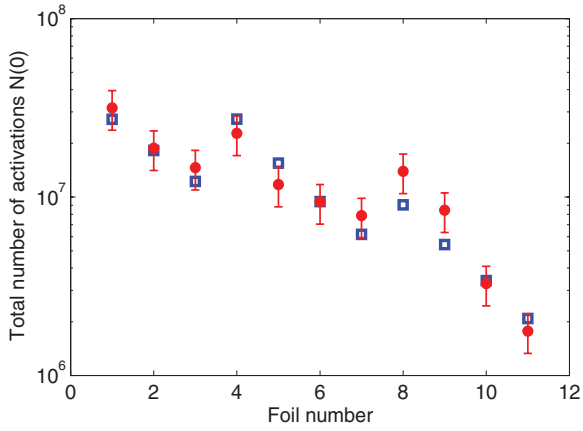

FIG. 8. Nuclear activations per copper foil. The red dots are reaction yields obtained from autoradiography of copper foils. The blue boxes show the calculated reaction yields using the exponential fit (see text). The steps at foil numbers 4 and 8 result from the different thicknesses (50, 130, and 260 μm) of foils within the stack.

A better description of the proton spectrum can be obtained using a modified exponential spectrum by Fuchs *et al.*[20]

$$\frac{dN_p}{dE} = \frac{N_{p,0}}{\sqrt{2E_p k_B T}} \exp\left(-\sqrt{\frac{2E_p}{k_B T}}\right). \tag{13}$$

The initial proton number N_0 and the slope $k_B T$ have to be determined, only, where k_B is the Boltzmann constant, and T is related to the average velocity of the protons. These parameters and therefore the proton spectrum can be determined by the least squares method using Eq. (11). Equation (11) transposes to

$$0 = \sum_b Q_{b,k} \frac{dN_p}{dE}(\bar{E}_{b,0}) \frac{\Delta \bar{E}_{b,0}}{Y(k)} - 1. \tag{14}$$

The squaring and summation above the kth foils lead to the basic equation for the numerical deconvolution of the parameters N_0 and $k_B T$ using the least square fit routine

$$0 = \sum_k \left(\sum_b Q_{b,k} \frac{dN_p}{dE}(\bar{E}_{b,0}) \frac{\Delta \bar{E}_{b,0}}{Y(k)} - 1 \right)^2. \tag{15}$$

The right of Eq. (15) is minimized with the consideration of a exponential proton spectrum using a numerical procedure by MATLAB.[18] The results of the fit are the parameters N_0 and $k_B T$. In addition, we can calculate theoretically the number of activations in each layer. The comparison between the theoretical reaction yields and the determined reaction yields in each copper layer is shown in Fig. 8. The different levels in the yield at foil numbers 4 and 8 can be explained by the different foil thicknesses. There is a good agreement between the yield calculated by the fit, and the reaction yield determined by the autoradiography. Furthermore, we can use the fit method to deconvolve the proton spectrum.

For comparison of NAIS with RIS, we used alternating stacked layer of RCFs and copper. For the deconvolution of the proton spectrum, we used the method described by Nürnberg *et al.*[13] An example shown in Fig. 9 describes both, one proton spectrum obtained from NAIS and one from RIS. The

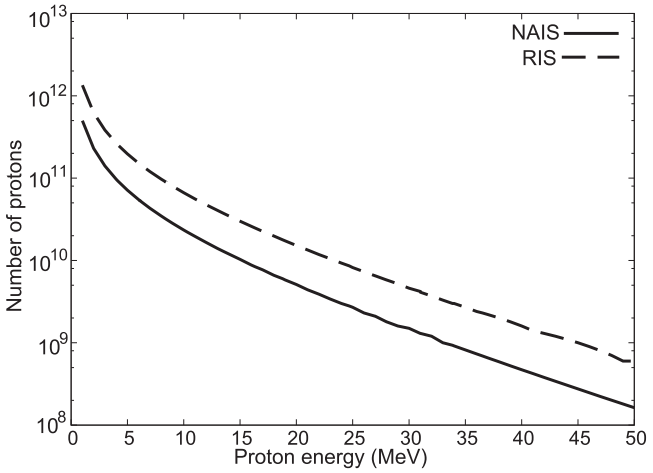

FIG. 9. Comparison of both proton spectra obtained from NAIS and RIS.

result is that the numbers of protons are different regarding NAIS and RIS. This can be explained by the error of the absolute calibration of the RCFs which is more than 35%. The overall error together with the error of the analysis method is around 50%. Using NAIS we get an error of around 35%. That means there is an overlap between the error bounds of the absolute numbers of protons obtained from NAIS and RIS. In summary, within the accuracy of both methods the absolute numbers of protons obtained from NAIS and RIS are in nice agreement.

IV. CONCLUSION

In conclusion, we presented a NAIS for the investigation of laser generated high flux proton beams. An autoradiography of activated copper foils using IP detectors was performed to reconstruct the spectrally and spatially resolved beam profile. The main part is the calibration method of the IPs. We prefer a cross-calibration technique using well known nuclear physics detection methods such as coincidence counting systems and gamma spectroscopy. The result is together with the efficiency of the used IP type, the relation between the PSL value, and the absolute number of laser generated protons per energy bin. Furthermore, the comparison of NAIS with the more established RIS method has shown the capability of NAIS to reconstruct the beam profile with high spectral and spatial resolution.

In summary, there are some advantages of NAIS as an imaging diagnostics tool. Compared to other diagnostics, NAIS can be used without saturation effects for the imaging of high energy and high flux proton beams generated in high power single shot laser applications. More sophisticated detectors are based on scintillators or semiconductors and can be used as online diagnostics in multishot laser applications. However, these detectors are limited for high flux particle beams and sensitive to the intense X-ray flash, which appears in laser-matter interactions. In addition, using foils of other materials than copper, NAIS can be extended to investigate other particle beams besides protons such as neutrons and deuterons depending on the nuclear reaction cross section.

ACKNOWLEDGMENTS

The work of M.M.G., K.H., G.H., A.O., F.N., A.P., and M.R. was supported by BMBF (Federal Ministry of Education and Research), support codes 06DA9043I, 06DA9044I, and 05KS7SJ1.

[1]M. D. Perry and G. Mourou, Science **264**, 917 (1994).
[2]S.-W. Bahk *et al.*, Opt. Lett. **29**, 2837 (2004).
[3]M. M. Günther, K. Sonnabend, E. Brambrink, K. Vogt, V. Bagnoud, K. Harres, and M. Roth, Phys. Plasmas **18**, 083102 (2011).
[4]K. B. Wharton, S. P. Hatchett, S. C. Wilks, M. H. Key, J. D. Moody, V. Yanovsky, A. A. Offenberger, B. A. Hammel, M. D. Perry, and C. Joshi, Phys. Rev. Lett. **81**, 822 (1998).
[5]J. J. Santos, F. Amiranoff, S. D. Baton, L. Gremillet, M. Koenig, E. Martinolli, M. Rabec Le Gloahec, C. Rous-Seaux, D. Batani, A. Bernardinello, G. Greison, and T. Hall, Phys. Rev. Lett. **89**, 025001 (2002).
[6]F. Brandl, G. Pretzler, D. Habs, and E. Fill, Europhys. Lett. **61**, 632 (2003).
[7]T. W. Phillips, M. D. Cable, T. E. Cowan, S. P. Hatchett, E. A. Henry, M. H. Key, M. D. Perry, T. C. Sangster, and M. A. Stoyer, Rev. Sci. Instrum. **70**, 1213 (1999).
[8]I. Spencer, K. W. D. Ledingham, R. P. Singhal, T. McCanny, P. McKenna, E. L. Clark, K. Krushelnick, M. Zepf, F. N. Beg, M. Tatarakis, A. E. Dangor, M. A. Norreys, P. A. Edwards, R. D. Sinclair, R. J. Clark, and R. M. Allot, Rev. Sci. Instrum. **73**, 3801 (2002).
[9]S. P. Hatchett *et al.*, Phys. Plasmas **7**, 2076 (2000).
[10]L. Yin, B. J. Albright, B. M. Hegelich, K. J. Bowers, K. A. Flippo, T. J. T. Kwan, and J. C. Fernández, Phys. Plasmas **14**, 056706 (2007).
[11]A. Henig *et al.*, Phys. Rev. Lett. **103**, 245003 (2009).
[12]D. S. Hey, M. H. Key, A. J. Mackinnon, A. G. MacPhee, P. K. Patel, R. R. Freeman, L. D. Van Woerkom, and C. M. Castaneda, Rev. Sci. Instrum. **79**, 053501 (2008).
[13]F. Nürnberg, M. Schollmeier, E. Brambrink, A. Blazevic, D. C. Carroll, K. Flippo, D. C. Gautier, M. Geißel, K. Harres, B. M. Hegelich, O. Lundh, K. Markey, P. McKenna, D. Neely, J. Schreiber, and M. Roth, Rev. Sci. Instrum. **80**, 033301 (2009).
[14]J. Metzkes *et al.*, Rev. Sci. Instrum. **83**, 123301 (2012).
[15]M. Tarisien, C. Plaisir, F. Gobet, F. Hannachi, M. M. Aléonard, and A. Rebii, Rev. Sci. Instrum. **82**, 023302 (2011).
[16]See http://www-nds.iaea.org/exfor/exfor.htm for EXFOR experimental nuclear reaction database.
[17]J. M. Yang, P. McKenna, K. W. D. Ledingham, T. McCanny, S. Shimizu, L. Robson, R. J. Clark, D. Neely, P. A. Norreys, M.-S. Wei, K. Krushelnick, P. Nilson, S. P. D. Mangles, and R. P. Singhal, Appl. Phys. Lett. **84**, 675 (2004).
[18]See http://www.mathworks.de/products/matlab/ for more information about the numerical computation system MATLAB.
[19]A. S. Penfold and J. E. Leiss, Phys. Rev. **114**, 1332 (1959).
[20]J. Fuchs *et al.*, Nat. Phys. **2**, 48 (2006).
[21]J. F. Ziegler, Nucl. Instrum. Methods Phys. Res. B **219–220**, 1027 (2004).